CONSTRAINING THE HIGH DENSITY NUCLEAR SYMMETRY ENERGY WITH PIONS

By

Justin Estee

A DISSERTATION

Submitted
to Michigan State University
in partial fulfillment of the requirements
for the degree of

Physics – Doctor of Philosophy

2019

ABSTRACT

CONSTRAINING THE HIGH DENSITY NUCLEAR SYMMETRY ENERGY WITH PIONS

By

Justin Estee

ACKNOWLEDGEMENTS

Your acknowledgements here.

TABLE OF CONTENTS

LIST OF TABLES vii

LIST OF FIGURES viii

CHAPTER 1 INTRODUCTION 1
- 1.1 From Nuclear Forces to the Equation of State 1
- 1.2 Phases of Nuclear Matter 1
- 1.3 The Nuclear Equation of State 1
- 1.4 Previous Constraints 1
- 1.5 Motivation for building the SπRIT TPC 1

CHAPTER 2 THEORY 2
- 2.1 From Nuclear Forces to Equation of State 2
- 2.2 Nuclear Equation of State 2
- 2.3 Boltzmann Ulong Uhlenbeck (BUU) Transport Code 2
- 2.4 Observables 2
- 2.5 The π observable 2

CHAPTER 3 EXPERIMENT 3
- 3.1 SπRIT TPC Overview 3
- 3.2 Considerations when constructing a TPC 4
- 3.3 Field Cage 5
- 3.4 Voltage Step Down 6
- 3.5 Wire Planes 6
- 3.6 Pad Plane 6
- 3.7 Electronics 6
- 3.8 SπRIT at RIBF 7
- 3.9 Kyoto Multiplicity Trigger 7
- 3.10 Krakow ?????? (KATANA) 7
- 3.11 Ancillary Detectors 7
- 3.12 Radio Isotope Beam Factory (RIBF) Facility 7
- 3.13 Experimental setup 8
- 3.14 Trigger Condition 8

CHAPTER 4 DATA ANALYSIS I: CALIBRATION AND CORRECTIONS 9
- 4.1 Software 9
- 4.2 Calibrations 12
- 4.3 Corrections 12
- 4.4 Monte Carlo Simulation 13
- 4.5 Drift Task 13
- 4.6 Pad Response Task 14
- 4.7 Electronics Task 15

4.8 Track Embedding 15
4.9 Efficiency Corrections 16

CHAPTER 5 DATA ANALYSIS II: EXTRACTING PHYSICS 6
5.1 Beam Particle Identification 6
5.2 Event Mixing 6
5.3 Reaction Plane Determination 6

CHAPTER 6 RESULTS 7
6.1 Comparison to Theory 7
6.2 π Yields 7
6.3 π^-/π^+ Ratio 7
6.4 Constraint on the Symmetry Energy 7

APPENDIX 8

BIBLIOGRAPHY 10

LIST OF TABLES

Table 3.1 An overview of the properties of the SπRIT TPC. 4

Table 3.2 Summary of the optional settings of the GET electronics and those used during the 20?????? experimental runs 7

LIST OF FIGURES

Figure 3.1 Exploded view of the SπRIT TPC 5

Figure 3.2 Overview of the RIBF, BigRIPS, and SAMURAI beamline. 8

Figure 4.1 Cartoon graphic of a top down view of a fit to a track passing through several pads. The bolded pads and the charges q_i represent the hits belonging to that pad and the clusters of the track representing the average position of the track. The three clusters at the bottom are clustered in the x-direction and for the upper three clustered in the z-direction. The estimate of the position of the avalanche is given by the track fit and the position from the center to each pad to the $\bar{x}$ position is given as λ_i. 11

Figure 4.2 A cartoon illustration of the charge distribution resulting from an electron avalanche on one wire and the projections of the distribution onto the two axis $\rho(x)$ onto the x-axis and $\rho(z)$ onto the z-axis. The orientation of the wire planes is flipped upside down to display the perspective better. 12

Figure 4.3 A summary of all the effects modeled in the TPC MC simulation. 13

Figure 4.4 A cartoon of the wires over one pad. 14

Figure 4.5 Comparison of MC and data PRF 15

CHAPTER 3

EXPERIMENT

3.1 SπRIT TPC Overview

The Samurai Pion-Reconstruction and Ion Tracker Time Projection Chamber (SπRI TPC) is a Multi-Wire Proportional Counter developed to measure pions and other light charge particles resulting from radioactive heavy ion collisions in a fixed target experiments. The TPC is enclosed in a thin aluminum sheet walls all around in order to minimize neutron scattering and to allow for light charged particles to reach the arrays of scintillating bars detectors on the sides and downstream of the TPC. The SπRI TPC was developed to fit inside the Samurai dipole magnet used at the Rare Isotope Beam Factory (RIBF) at RIKEN in Wako-shi, Japan [1]; the dipole gap limited the vertical space of the TPC. More detail and specifications of the Samurai dipole magnet are given in [2].

A target ladder allowed for up to 5 fixed targets to be mounted. A ACME worm gear allowed for the x-axis motion for changing the targets. The motion of this worm gear was translated through the target motion feed-through by several brass gears and non-magnetic gear boxes. The motion of the target ladder could be controlled by hand or by operation of the drill. The targets were mounted on stand-offs on the target ladder and also had z-axis motion. This allowed for the targets to be positioned as close as possible to the thin window of the field cage, maximizing the geometric acceptance.

The electronics were mounted to the aluminum top plate. Several aluminum ribs were mounted to the top of the plate to bring structural rigidity. Because of this the top plate flatness was within 150μm across the whole top plate as measured by a laser position system. The charge sensitive pads of the pad plane were etched into several circuit boards were recessed and glued to the bottom portion of the top plate. Vias through the pad plane circuit boards brought the signal traces from the pads to surface mount pads on the other side of the boards. Several holes cut through the top plate allowed for the interface cables of the electronics to be connected to these surface pads.

SπRIT TPC Overview			
Pad Plane Area	1.3 m x 0.9 m	Gas Gain	1000
Pad Size	1.2 cm x 0.8 cm	Drift Velocity	5.5 cm/μs
Number of pads	12096 (112x108)	E-field	135 V/cm
Gas composition	90% Ar + 10% CH_4	Multiplicity limit	200
Drift length	50 cm	dE/dx range	Z=1-8, π, p,d,t,He,Li-O

Table 3.1 An overview of the properties of the SπRIT TPC.

Just below the pad plane were a set of three wire planes; the gating grid, ground, and anode wire planes. The detailed function of these wires will be explained later but they served to separate the boundary between the drift volume and the avalanche volume.

The front and sides of the field cage were assembled from 8 independent rigid circuit boards. The downstream window served as the downstream wall of the field cage all though it was was a large polycarbonate frame in which a removable kapton window could be installed. This thin window minimized the scattering of exiting neutrons and charged particles for downstream detectors.

The voltage step down takes the high voltage of the field cage cathode and steps the voltage down through a set of copper rings and a resistor chain, minimizing the chance for sparking.

3.2 Considerations when constructing a TPC

Several considerations went into the construction of the SπRI TPC which I wish to summarize and document here. All materials and glue of the TPC were selected as low out-gassing materials. Several materials that are common place in nuclear labs, from vacuum grease to o-rings, out-gas organic chemicals into the counter gas which damage the TPC by permanently lowering the gain over time. The organic molecules responsible are difficult to identify exactly, but lists of good and bad materials are well known in the literature from experiments. If a material we wished to used was not on these lists we placed the material in a clean chamber with the counter gas and flowed this counter gas through a small proportional counter making sure the gain did not drop at high collection rates when exposed to a high rate alpha Americium source.

Sparking Two volumes of gas.

3.3 Field Cage

The field cage was designed to hang from the top plate and therefore needed to be of a lightweight construction. Also the materials needed to be thin to allow for light charged particle and neutrons to pass through without significant scattering for ancillary detectors. Therefore instead of a downstream wall, a large thin exit window was constructed. The cathode was constructed of an aluminum honeycomb laminate. Two sheets of ??? aluminum were bonded to a core of aluminum honeycomb structure providing a lightweight yet rigid structure for the cathode.

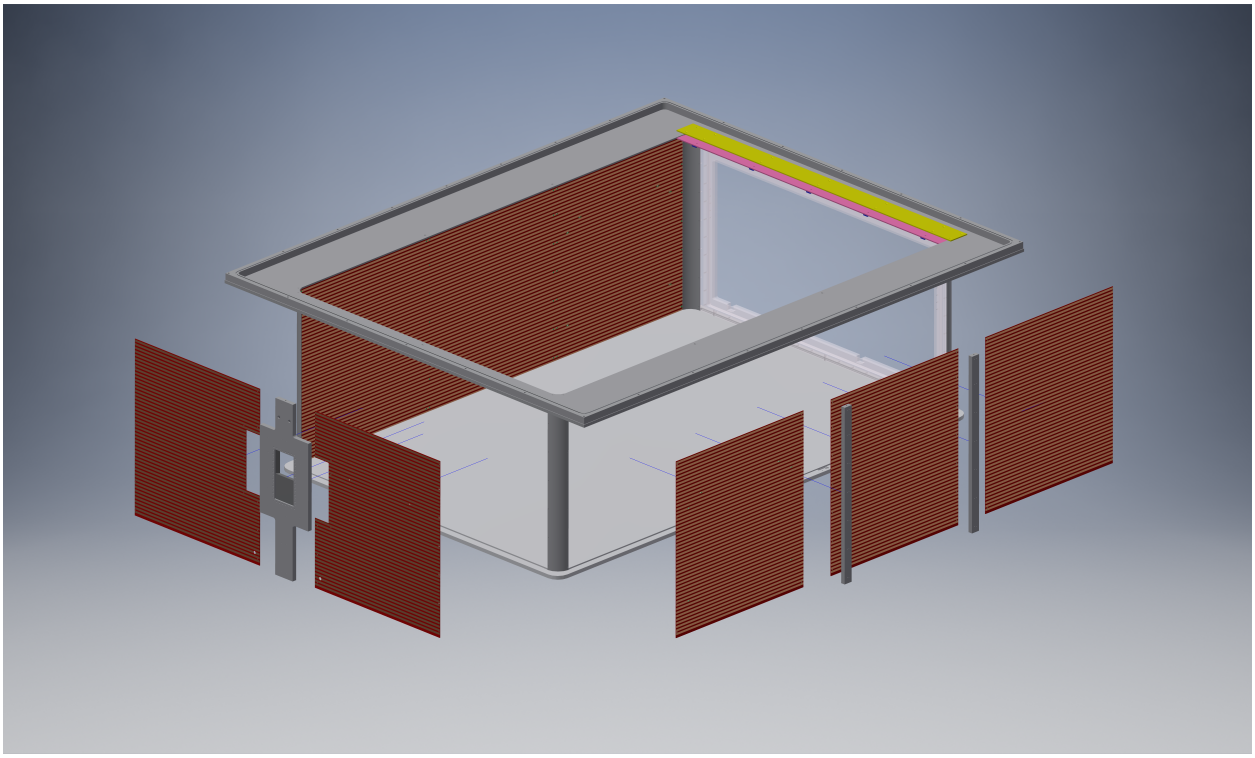

Figure 3.1 Exploded view of the SπRIT TPC

The field cage was constructed from several panels of printed circuit boards (PCBs). The epoxy in the common PCB substrate FR4 contains bromine which is not suitable for the long term operation of a TPC, as the bromine will eventually cause gain reduction of the wires [CITE]. The

halogen free material chosen was Rodgers ????. We build the TPC with the option to run explosive gases such hydrogen, thus we decided to have field cage an isolated volume from the rest of the TPC enclosure. While the risk of a high voltage spark was minimized using the voltage step down, the risk of sparking when using an explosive gas could be further minimized by isolating the detector volume from the enclosure volume thereby allowing you to run an insulating gas between the field cage while running the explosive gas inside the detector volume only.

The front of the field cage was made of two PCBs and each side was constructed of three PCBs. The exit window was a 10μm thick Kapton window with evaporated aluminum strips on the inside and outside; mounted on a polycarbonate frame.

3.4 Voltage Step Down

To lower the risk of a high voltage spark around the cathode region a voltage step down was developed. A series of 7 concentric copper rings with 20 MOhm resistors between them steps the cathode voltage down to ground. This minimizes sharp transitions of the electric field and therefore sparking.

3.5 Wire Planes

3.6 Pad Plane

3.7 Electronics

Signals in the SπRIT TPC are amplified and digitized by the recently developed Generic Electronics for TPCs (GET) [3]. Short cables transmit the signals from the pads to the inputs of the AGET chips. Each AGET chip services 64 pads (63 pads are connected in our case), contains a pre-amplifier, and a Switched Capacitor Array (SCA), with a maximum of 512 time buckets with an adjustable sampling frequency of 1 to 100 MHz. Four AGET chips are mounted on one AsAd (ASIC and

GET Electronics Settings			
GET settings	All options	^{132}Sn + ^{124}Sn	^{124}Sn + ^{112}Sn
ADC bit range	14 bits		
Sampling frequency	1 - 100 MHz		
Dynamic range	.12,.24,1.0,10 pC		
Peaking time	69,117,232,501,720, 1014 ns		
Time bucket	512	270	270

Table 3.2 Summary of the optional settings of the GET electronics and those used during the 20?????? experimental runs

ADC) motherboard. The gain of each AGET can be configured as 0.12, 0.24, 1.0, or 10 pC over the whole dynamic range, and the ADCs on each AsAd board provides 12 bit resolution. The peaking times of the shaping amplifiers can be set to 69, 117, 232, 501, 720, or 1014 ns. In this experiment, the gain was set to the highest setting, 0.12 pC, the peaking time 117 ns, and the sampling frequency 25 MHz (resulting in 40 ns time buckets). The Aget 2.0, asad 2.1, and cobo 1.0 firmware versions were used. The variations in the electronics were calibrated by measuring the response of each channel to a injected reference pulse, covering the full dynamic range of each channel.

3.8 SπRIT at RIBF

3.9 Kyoto Multiplicity Trigger

3.10 Krakow ?????? (KATANA)

3.11 Ancillary Detectors

3.12 Radio Isotope Beam Factory (RIBF) Facility

SAMURAI (Superconducting Analyzer for Multi-particles from Radioisotope beams) is a large-acceptance multi-particle spectrometer for radioactive-beam experiments.

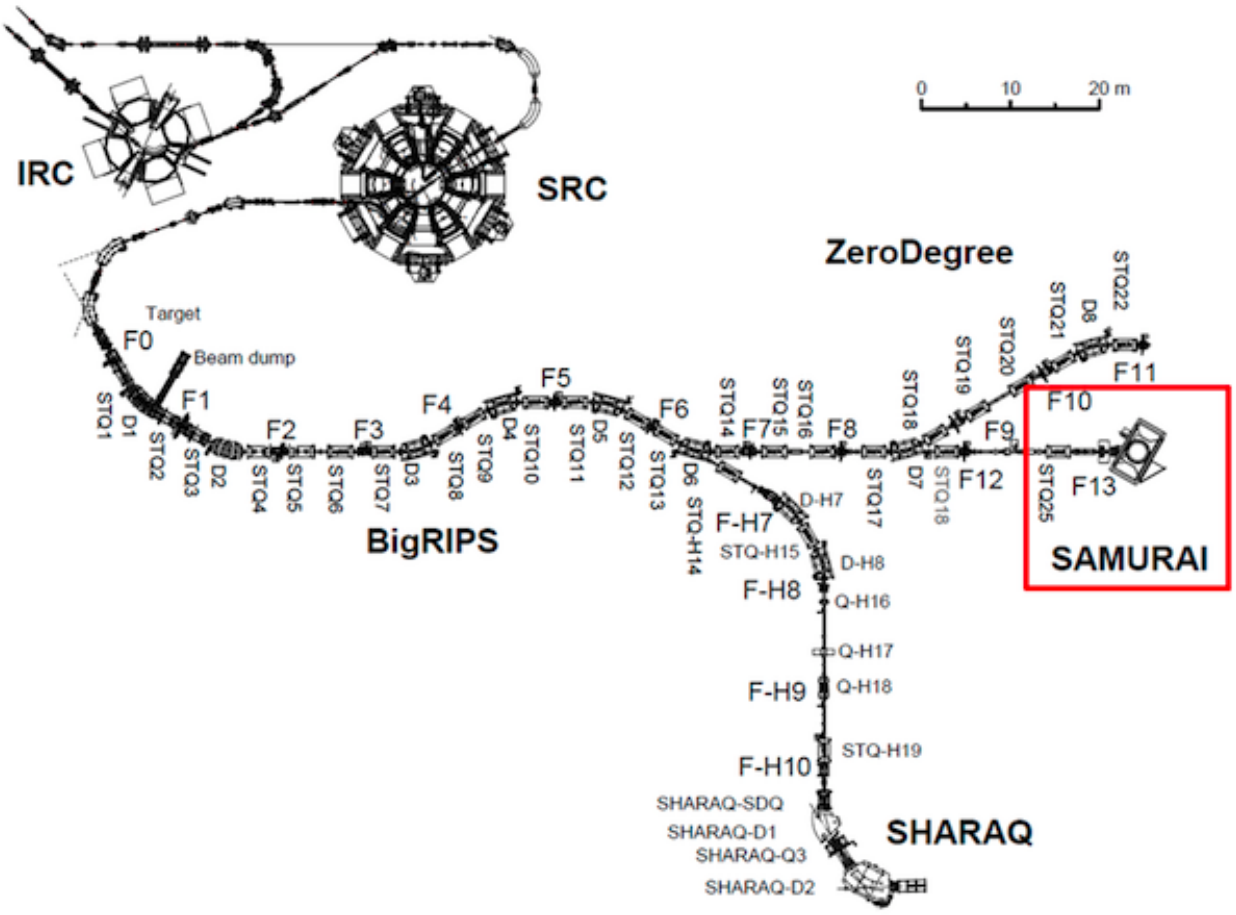

Figure 3.2 Overview of the RIBF, BigRIPS, and SAMURAI beamline.

3.13 Experimental setup

3.14 Trigger Condition

CHAPTER 4

DATA ANALYSIS I: CALIBRATION AND CORRECTIONS

4.1 Software

The SπRITROOT software is modular tasked based code based on the FAIRROOT package written in C++ [4]. The main tasks in the SπRITROOT software reconstruction are:

- Decoder task
- Pulse Shape Algorithm (PSA Task)
- Helix Track Finding Algorithm
- Clustering Algorithm
- Track Fitting (GENFIT package)
- Vertex Fitting (RAVE package)

The decoder task converts the binary data file into a container class which maps the electronics channels into the corresponding pads and (x,z) coordinates.

There may be several pulses in a pad coming from two tracks passing under the same pad separated by arrival time. Using an expected pulse shape the PSA task fits the signal pulses within a pad, giving the arrival time of the drifted electrons from each particular track. The height of the fitted pulse is proportional to the total charge of that event, Q and the y-coordinate is calculated as $y = v \cdot t_0$ where v is the drift velocity and t_0 the arrival time. Combining the information from these first two tasks, (x,y,z,Q), we construct what is called a "hit".

The Helix Track Finding Algorithm finds the collection of hits belonging to one track out of all the hits in an event. The hits within a track are then reduced into clusters. A cluster's position is the average position of the hits within a cluster, with the total charge of the cluster being the sum of the hits charges.

A tracks average position is estimated by the cluster's average position. The clusters are then fitted in the GENFIT track fitting package [5], giving the final momentum of the track. A final vertex of the event is fitted from all tracks using the package RAVE [6].

Definition of clustering A brief description of the method of clustering is illustrated in Figure 4.1. It is impractical to cluster in both the x and z-axis and we only cluster the hits along one axis. The three clusters at the bottom of Figure 4.1 are clustered along the x-axis and the upper three are along the z-axis, as shown by the bolded pads for one of the clusters in each direction.

The clustering direction depends on the angle of the track with respects to the x-axis, defined as θ. For example, a track going along the z-axis the crossing angle is defined as 90°, and a track going along the x-axis defined as 0°. In the case that the crossing angle is $45^\circ < \theta \leq 90^\circ$ the clustering direction is along the x-axis. For $0^\circ < \theta \leq 45^\circ$ it is along the z-axis.

The position along the clustering direction is calculated by weighting the individual hit's positions by their charges q_i and getting the mean value. The other direction is set to the center of the pad. For example if we are clustering along the x-axis for a cluster, the z-position is set to the center of the pad in the z-direction and vice versa.

Clustering in this way gives us better position resolution for calculating the position of each cluster. You could imagine if we calculated the clusters only along the x-axis for tracks with $\theta \approx 0^\circ$ the x-position is not well defined. By clustering in the direction most perpendicular to the track, we get a better position resolution.

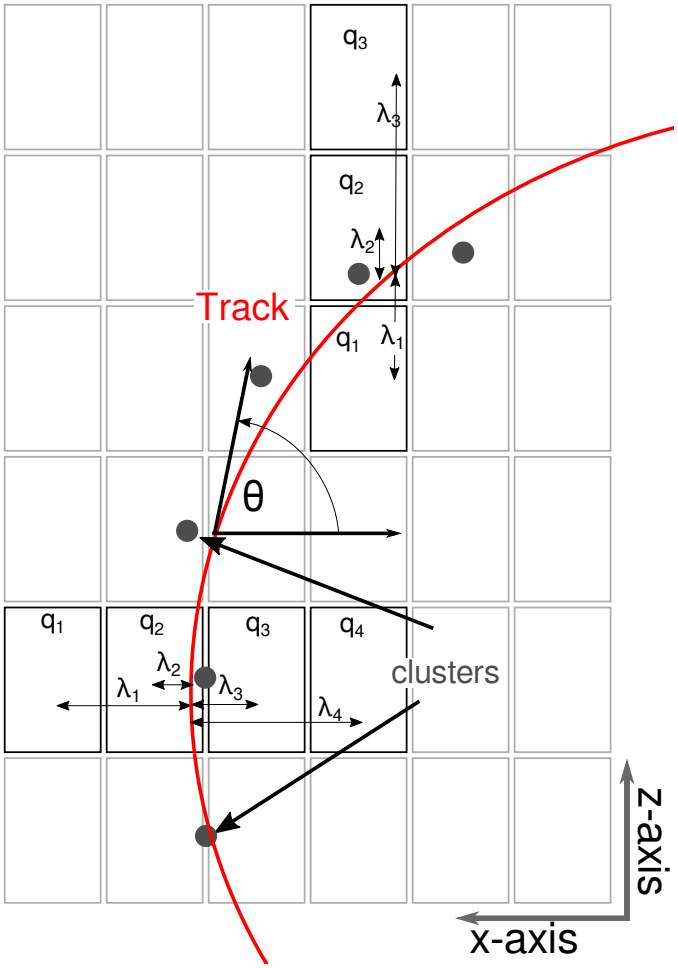

Figure 4.1 Cartoon graphic of a top down view of a fit to a track passing through several pads. The bolded pads and the charges q_i represent the hits belonging to that pad and the clusters of the track representing the average position of the track. The three clusters at the bottom are clustered in the x-direction and for the upper three clustered in the z-direction. The estimate of the position of the avalanche is given by the track fit and the position from the center to each pad to the $\bar{x}$ position is given as λ_i.

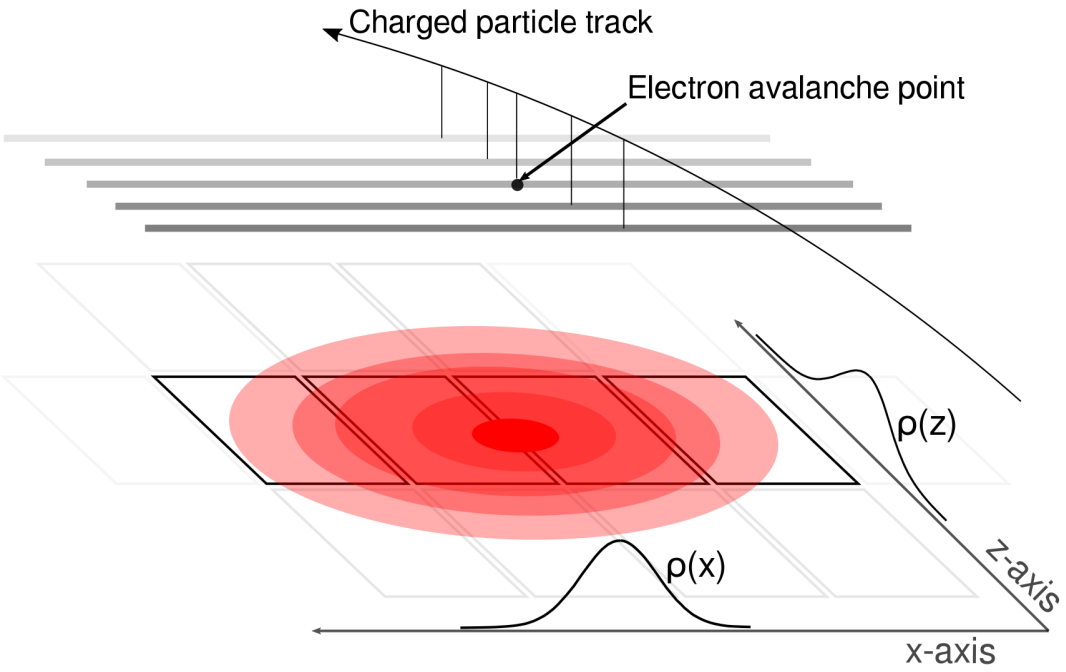

Figure 4.2 A cartoon illustration of the charge distribution resulting from an electron avalanche on one wire and the projections of the distribution onto the two axis $\rho(x)$ onto the x-axis and $\rho(z)$ onto the z-axis. The orientation of the wire planes is flipped upside down to display the perspective better.

4.2 Calibrations

Electronics calibration

Anode gain calibration

4.3 Corrections

Extending the dynamic range of Electronics

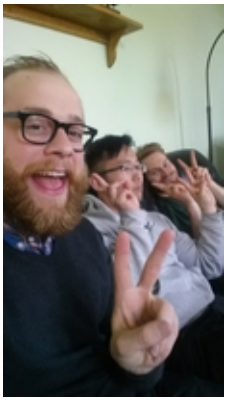

Figure 4.3 A summary of all the effects modeled in the TPC MC simulation.

4.4 Monte Carlo Simulation

We use Geant4 as and event generator for performing Monte Carlo Simulations in the TPC. A scale model of field cage, front window, front window frame, pad plane, and aluminum top plate are modeled. The correct materials are used as well as the field cage is modeled with P-10 gas at a density of ????. By using Geant4 we can also input the the magnetic field map of the SAMURAI dipole magnet (as calculated by the SAMURAI group via a TOSCA simulation). In this way any particle type may be studied and the full interactions (scattering, decay, energy loss, path taken, etc.), are accounted for. The output of this simulation is a series of energy loss points which contain the amount of energy lost in keV/cm and the position in (x, y, z).

Separate software tasks model the converting energy loss into electrons, the drifting of electrons, the avalanche process, and the electronics response.

4.5 Drift Task

The drift task takes the energy loss points calculated from Geant4 and converts them into electrons. and then modeling their drift behavior in the field cage. As discussed previously the various processes[CITE To formula about drifting electronc]

A full microscopic treatment of the stochastic nature of each electron would be too cumbersome;

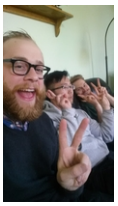

Figure 4.4 A cartoon of the wires over one pad.

most of the properties of the electrons are described by macroscopic quantities can be described by The charge of each MC point is converted to the total number of electrons liberated in the P-10 gas. This is a well understood property of proportional counters and is stable over a wide range of velocities and particle types [CITE BOOK]. The conversion factor of P-10 can be calculated by considering the partial volumes of each component of the gas. 4.1.

$$Numberofe^{-} = 28keV/cm \tag{4.1}$$

4.6 Pad Response Task

After the avalanche process of the previous task, the total charge of the event is split over several pads defined by the Pad Response Function (as discussed in section ????). As shown in Fig. 4.4, there are three wires that lie directly above a given pad. The z coordinate of the avalanche can only be one of these three wires, where as the x coordinate can be any value along the wire. The functional form of the software PRF (given in Eq. 4.2), was tuned to match the experimental data. Shown in Fig. 4.5, we see the tuned software PRF can match the experimental PRF from data over several crossing angles (as mentioned in Chapter ???? governs the shape of the PRF).

$$PRF(x,z) = \frac{1}{2\pi\sigma_z\sigma_x} \exp^{\frac{-(x-x_O)^2}{2\sigma_x^2}} \exp^{\frac{-(z-z_O)^2}{2\sigma_z^2}} \tag{4.2}$$

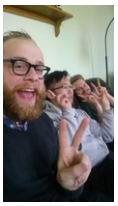

Figure 4.5 Comparison of MC and data PRF

4.7 Electronics Task

The electronics task takes the total charge on each pad and simulates the electronics response, converting electronics into ADC channels. Accounting for the pedestal, the measured output in ADC channels (for a given gain setting) is given in Eq. 4.3.

$$1\text{ADC} = \frac{ADC_{\text{Max}} - ADC_{\text{Pedestal}}}{G * f_c} \tag{4.3}$$

4.8 Track Embedding

Track embedding is the process of taking a MC track from Geant4 and embedding that simulated response into a real data event, reconstructing this event, and matching the input MC track to its final measured value. By doing so we can evaluate the response of the entire TPC system to any input value given. The TPC system is composed of three major components, each which can introduce errors and or biases, the software, the measurement, and the experimental setup.

Analyzing the response of the software is the most straight forward; let the software routine process an input and measure the result. Understanding the measurement requires modeling the physics involved in the theory and operations of TPC's and the electronics. The experimental setup itself is quite large and complex, several ancillary detectors such as the Kyoto multiplicity array, Krakow veto array, Active veto array, beam identification detectors, etc. Even if a full accurate model could be constructed the complex trigger logic of the DAQ system would be impossible to model. If we notice that the biases and errors of the entire experimental setup is contained in the

measured experimental data. Therefore, by inputting the MC data into a real experimental event (and measuring the output of that MC track) we can estimate the errors of the experimental setup.

The software analysis routine and the bias introduced by the trigger settings of the experiment introduce systematic errors in the reconstruction of tracks

4.9 Efficiency Corrections

Since the SπRIT TPC is a fixed target experiment it's angular coverage is certainly not 4π. Because the target is several cm away from the widow of the field cage the geometric acceptance is not even 2π. The rectangular design complicates the calculation of the geometric acceptance, or the efficiency.

APPENDIX

APPENDIX

YOUR APPENDIX

BIBLIOGRAPHY

BIBLIOGRAPHY

[1] Y. Yano, he ri beam factory project: A status report, Nucl. Instrum. Meth. B 261 (1-2) (2007) 1009–1013. doi:10.1016/j.nimb.2007.04.174.

[2] T. K. et. al., Samurai spectrometer for ri beam experiments, Nucl. Instrum. Meth. B 317 (2013) 294–304. doi:10.1016/j.nimb.2013.05.089.

[3] E. P. et. al., Get: A generic and comprehensive electronics system for nuclear physics experiments, Physics Procedia 37 (2012) 1799–1804. doi:10.1016/j.phpro.2012.02.506.

[4] M. A.-T. et. al., The fairroot framework, J. Phys.: Conf. Ser. 396 (2). doi:10.1088/1742-6596/396/2/022001.

[5] C. H. et. al., A novel generic framework for track fitting in complex detector systems, Nucl. Instrum. Meth. A 620 (2-3) (2010) 518–525. doi:10.1016/j.nima.2010.03.136.

[6] W. Waltenberger, Rave—a detector-independent toolkit to reconstruct vertices, IEEE Transactions on Nuclear Science 58 (2) (2011) 434–444. doi:10.1109/TNS.2011.2119492.